

THEORETICAL AND EXPERIMENTAL NONLINEAR DYNAMICS OF A CLAMPED-CLAMPED BEAM MEMS RESONATOR

Rob M. C. Mestrom, Rob H. B. Fey, Henk Nijmeijer

Department of Mechanical Engineering
Eindhoven University of Technology
the Netherlands

R.M.C.Mestrom@tue.nl, R.H.B.Fey@tue.nl, H.Nijmeijer@tue.nl

Abstract

Microelectromechanical resonators feature nonlinear dynamic responses. A first-principles based modeling approach is proposed for a clamped-clamped beam resonator. Starting from the partial differential equation for the beam including geometric and electrostatic nonlinear effects, a reduced-order model is derived. The model captures the experimentally observed nonlinear dynamic behaviour of the resonator and allows for fast simulation and prediction of its response.

Key words

MEMS resonator, first-principles based modeling, steady-state nonlinear dynamics, experiments

1 Introduction

Single-crystal microelectromechanical silicon resonators provide an interesting alternative for quartz crystals in oscillator circuits for modern data and communication applications (Nguyen, 2005, 2007). Their compact size, feasibility of integration with IC technology and low cost are major advantages. In oscillator circuits, nonlinearities in resonators influence oscillator performance. Conventional quartz crystal resonators are not driven into nonlinear regimes, since the rather bulky quartz crystal units can store sufficient energy for oscillation while remaining linear. However, MEMS resonators inherently can store less energy, due to their smaller size. For this reason, they have to be driven into nonlinear regimes in order to store enough energy for a sufficiently good signal to noise ratio (Kaajakari *et al.*, 2004). Depending on the specific resonator layout, different types of nonlinearities may be dominant in the resonator dynamic behaviour. The presence of the nonlinearities is relevant for oscillator performance and their analysis has to be incorporated in future resonator design optimization. In order to determine the influence of the different nonlinearities, the dynamic

behaviour of the resonator has to be understood. A predictive modeling approach which enables fast and accurate simulation of the nonlinear dynamics is essential for this.

The resonator under investigation here has a clamped-clamped beam layout. Various research groups have realized clamped-clamped beam resonators and have reported measurements, see for instance Mattila *et al.* (2002). However, a combined numerical and experimental analysis of the nonlinear behaviour of such a resonator has not been addressed extensively.

In this paper, a first-principles based approach will be proposed for modeling and analyzing the nonlinear dynamic behavior of clamped-clamped microelectromechanical beam resonators. In previous work (Mestrom *et al.*, 2007), based on a heuristic modeling approach (Kaajakari *et al.*, 2004), a match has been obtained between numerical and experimental results for a clamped-clamped beam resonator. Here, instead, a first-principles based modeling approach will be used, founded on partial differential equations (PDEs). Starting from the PDE, a reduced-order model will be derived, capturing essential nonlinear dynamic behavior of the resonator. The reduced-order model will be investigated using numerical tools for steady-state nonlinear dynamic analysis. This approach will allow for fast simulation and the investigation of nonlinear effects. Furthermore, it will potentially lead to more accurate prediction of the dynamic behavior than obtained so far (Mestrom *et al.*, 2007).

The outline of the paper is as follows. First, in Section 2, the resonator layout and some experimental results for a clamped-clamped beam resonator will be discussed. In Section 3, the modeling approach and the reduced-order model will be described. Simulation results from the model will be presented in Section 4 for some characteristic nonlinear dynamic effects. Finally, some conclusions will be drawn and an outlook to future work will be given in Section 5.

2 Clamped-Clamped Beam Resonator

A schematic drawing of the clamped-clamped beam resonator under investigation is depicted in Fig. 1. Herein, its characteristic flexural vibration shape is depicted as a dotted line. The actuation of the resonator is realized by means of a dc (V_{dc}) and an ac (V_{ac}) voltage component, which are applied to the two electrodes of the resonator by means of bias tees. The output of the resonator is measured as a voltage V_{out} , resulting from capacitive detection. This quantity can be related to the beam motion, see also Mestrom *et al.* (2007).

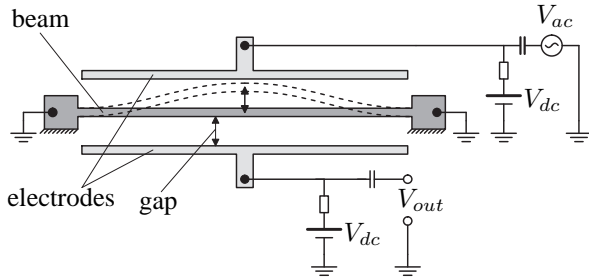


Figure 1. Schematic resonator layout.

The beam resonator has a length of $48 \mu\text{m}$, a width of $4 \mu\text{m}$ and a thickness of $1.4 \mu\text{m}$. The electrode gaps are 330 nm .

MEMS Resonators are fabricated using Silicon-On-Insulator (SOI) wafers. In the production process, first, aluminum bondpads are defined on the wafer surface. Next, the resonator layout is etched into the $1.4 \mu\text{m}$ thick SOI layer down to the buried oxide layer by means of deep reactive ion etching (DRIE). Finally, the resonator is released from the substrate through isotropic etching of the buried oxide layer using an HF wet etch solution. A microscope image of the clamped-clamped beam resonator is depicted in Fig. 2.

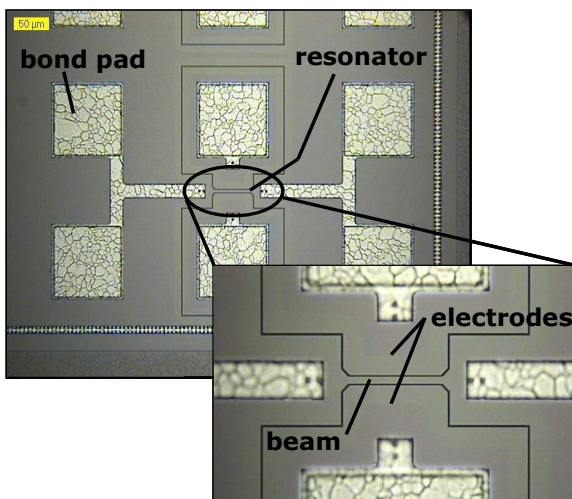


Figure 2. Microscope image of the resonator.

The grey material is silicon (Si, single-crystal), thin dark lines are lithography etch gaps and the white, grainy material corresponds to the aluminum (Al) bond pads and electrical lines. Six aluminum bond pads can be distinguished. These are designed in such a way that

they fit the ground-signal-ground probes that are used during the measurements. The outer four bond pads are connected to 'ground', such that the beam itself is grounded. The middle two bond pads are used for actuation and measurement purposes.

During the experiments, the MEMS resonator is located in a vacuum (pressure $p = 4.6 \times 10^{-4} \text{ mbar}$). Measurements of the steady-state dynamic behaviour of the resonator around the fundamental (first) natural frequency have revealed characteristic nonlinear dynamic behavior known as frequency hysteresis. By sweeping the excitation frequency up and down around the fundamental resonance frequency, an amplitude-frequency curve can be constructed. Two examples of such amplitude-frequency curves are depicted in Figs. 3 and 4, for ac excitation values of $V_{ac} = 70$ and 139 mV , respectively. In both cases, the bias voltage $V_{dc} = 70 \text{ V}$. The peak to peak value of V_{out} is depicted on the vertical axis.

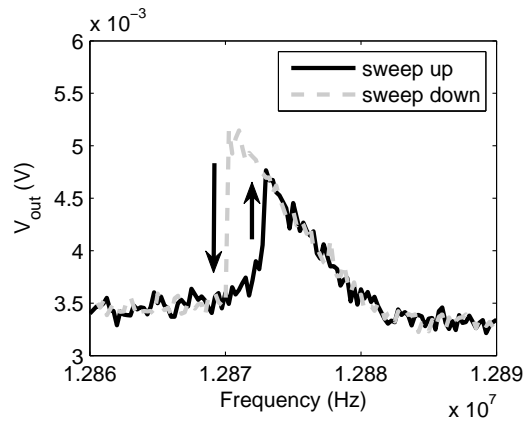


Figure 3. Experimental amplitude-frequency curve, $V_{ac} = 70 \text{ mV}$.

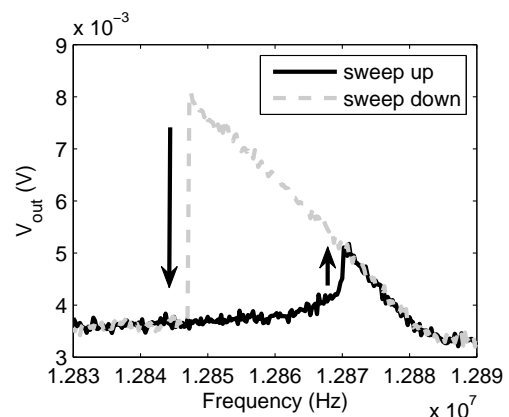


Figure 4. Experimental amplitude-frequency curve, $V_{ac} = 139 \text{ mV}$.

From these figures, it can be seen that the resonance frequency of the resonator is approximately 12.875 MHz . Moreover, the resonance peak bends to the left (lower frequencies) due to nonlinearities. As a result, the steady-state dynamic behaviour of the resonator is found to depend on the sweep direction. Sudden jumps in the response, indicated by black arrows,

occur at different frequencies. This typical nonlinear dynamic effect (frequency hysteresis) has also been reported in Kaajakari *et al.* (2004).

Another experimentally observed nonlinear dynamic effect is a $1/2$ subharmonic resonance, which occurs at twice the fundamental frequency, near 25.753 MHz. In a $1/2$ subharmonic resonance, the fundamental frequency in the system response is half the excitation frequency. The measured amplitude-frequency curve for $V_{dc} = 70$ V and $V_{ac} = 350$ mV is depicted in Fig. 5.

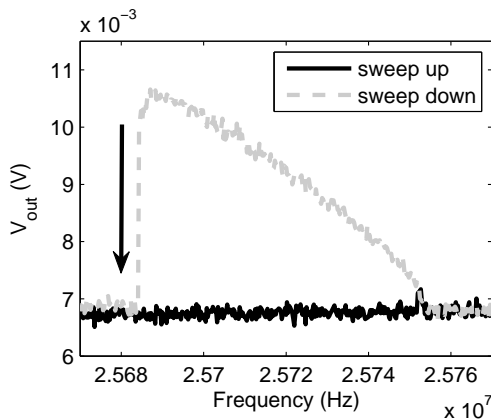


Figure 5. Experimental amplitude-frequency curve for the $1/2$ subharmonic resonance.

3 Modelling

The first-principles based modelling approach presented here, is an extension of recently reported work (Mestrom *et al.*, 2007) on the same resonator, where a heuristic single-degree-of-freedom model was proposed to capture experimentally observed behavior. The current approach will be founded on a partial differential equation for the beam, with electrostatic excitation.

Inherently, different physical domains are tightly intertwined at microscale (Senturia, 2001). At the moment, as a starting point for the modelling procedure, only structural mechanics and electrostatics have been included, so thermal effects and fluid damping have not been taken into account yet.

Underlying assumptions for the model that will be derived are the following. For now, fringing field corrections for the electrostatic actuation, see for instance Batra *et al.* (2006a) and Batra *et al.* (2006b), will not be included. Furthermore, several damping mechanisms may be present in micromechanical resonators (Foulogoc *et al.*, 2006), for instance, clamping losses, surface and bulk material losses, the already mentioned fluid (or squeeze film) damping and thermoelastic damping. For a description of thermoelastic damping see, for instance, Lifshitz and Roukes (2000) or Nayfeh and Younis (2004). In the current approach, these different damping mechanisms will be lumped into a single, equivalent linear damping parameter.

The effect and the accuracy of these assumptions will be addressed in future work.

3.1 Equation of Motion

For the case of flexural vibration of a clamped-clamped microbeam, consider the beam as depicted in Fig. 1. The beam is clamped on both sides and suspended between two stationary electrodes. The beam has a length l , a width b (out of plane) and a thickness h . A linear modelling approach for a beam with a single actuation electrode has already been reported in Tilmans *et al.* (1992) and Tilmans and Legtenberg (1994). This linear PDE is only valid for small transverse deformations of the beam. If deformations become larger, geometric nonlinear effects have to be considered. The type of effects depends on the type of resonator. For a clamped-clamped beam, large flexural deformations are accompanied by longitudinal stretching of the beam. This effect, also known as midplane stretching (Thomsen, 2003) results in axial tension in the beam, causing its effective stiffness to increase. Therefore, it corresponds to a hardening nonlinearity. Tilmans *et al.* (1992) calculated the resonance frequency of the beam, based on the Rayleigh quotient, including a correction for the potential energy change due to midplane stretching of the beam. An alternative method, described in Abdel-Rahman *et al.* (2002), and Younis and Nayfeh (2003), directly includes a nonlinear term in the partial differential equation to account for midplane stretching. This term appears in a similar way as an axial load N , resulting in the following equation:

$$EI \frac{\partial^4 w}{\partial x^4} + c \frac{\partial w}{\partial t} + \rho A \frac{\partial^2 w}{\partial t^2} = \left(N + \frac{EA}{2l} \int_0^l \left(\frac{\partial w}{\partial x} \right)^2 dx \right) \frac{\partial^2 w}{\partial x^2} + q(x, t). \quad (1)$$

Here, the transverse deflection $w = w(x, t)$ is a function of the coordinate x along the beam length and of time t . E equals the Young's modulus, ρ is the mass density and I and A denote the area moment of inertia and the beam cross-sectional area respectively. N denotes the tensile or compressive axial load present in the beam. In the following, the axial load is assumed to be zero, $N = 0$. In this paper, damping is accounted for by means of a damping constant c . This parameter can be seen as an equivalent linear damping parameter, although it is known that damping may very well depend on the excitation conditions for the resonator (see also Nayfeh and Younis, 2004). The second term on the right-hand side, $q(x, t)$, denotes the driving force per unit length, resulting from electrostatic excitation:

$$q(x, t) = \frac{1}{2} \frac{\epsilon_0 b}{(d-w)^2} V_1^2(t) - \frac{1}{2} \frac{\epsilon_0 b}{(d+w)^2} V_2^2, \quad (2)$$

where d denotes the gap width, constant ϵ_0 is the permittivity of free space and the excitation voltages are given by:

$$V_1(t) = V_{dc} + V_{ac} \sin(2\pi ft), \text{ and } V_2 = V_{dc}. \quad (3)$$

The current model for the electrostatic excitation (2) is a parallel plate approximation. The effect of fringing fields (see, for instance Batra *et al.*, 2006a) has not yet been included.

For a clamped-clamped beam, the boundary conditions of (1) consist of zero deflection and zero gradient at both clamped edges:

$$w(0, t) = w(l, t) = \frac{\partial w(0, t)}{\partial x} = \frac{\partial w(l, t)}{\partial x} = 0. \quad (4)$$

Material nonlinearities (higher-order elasticity effects) have not yet been included the current model.

3.2 Non-dimensional Equation of Motion

The equations describing the transverse deflection of the resonator (1), (2) and (3), can be written in non-dimensional form after scaling the position x , displacement w and time t as follows:

$$\bar{x} = \frac{x}{l}, \quad \bar{w} = \frac{w}{d}, \quad \bar{t} = t \sqrt{\frac{EI}{\rho Al^4}}. \quad (5)$$

As a result, spatial and temporal derivatives become:

$$\begin{aligned} (\dot{\cdot}) &= \frac{\partial}{\partial \bar{t}} = \sqrt{\frac{\rho Al^4}{EI}} \frac{\partial}{\partial t}, & (\ddot{\cdot}) &= \frac{\partial^2}{\partial \bar{t}^2} = \frac{\rho Al^4}{EI} \frac{\partial^2}{\partial t^2}, \\ (\cdot)' &= \frac{\partial}{\partial \bar{x}} = l \frac{\partial}{\partial x}. \end{aligned} \quad (6)$$

By using (5) and (6), the PDE for the beam (1) can be written as (for notational convenience, the bars, denoting non-dimensional quantities, have been omitted):

$$\begin{aligned} \ddot{w} + c_d \dot{w} + w^{(4)} - c_{nl} \left\{ \int_0^1 (w')^2 dx \right\} w'' = \\ c_f \left\{ \frac{V_1(t)^2}{(1-w)^2} - \frac{V_2^2}{(1+w)^2} \right\}, \end{aligned} \quad (7)$$

where damping parameter c_d (-), nonlinear stretching parameter c_{nl} (-) and voltage parameter c_f (V^{-2}) are given by:

$$c_d = c \sqrt{\frac{l^4}{\rho A EI}}, \quad c_{nl} = 6 \left(\frac{d}{h} \right)^2, \quad c_f = \frac{6\epsilon_0 l^4}{E d^3 h^3}. \quad (8)$$

The boundary conditions for (7) transform to:

$$w(0, t) = w(1, t) = w'(0, t) = w'(1, t) = 0. \quad (9)$$

3.3 Galerkin Discretization

The dynamic response of the system can be approximated in terms of a linear combination of a finite number of orthonormal spatial basis functions with time-dependent coefficients. This discretization (or separation of variables) procedure is often called the Galerkin procedure and is suited for both linear and nonlinear PDEs. For the microbeam resonator, the deflection $w(x, t)$ in (7) is expressed as a sum of spatial shapes that, a priori, satisfy the imposed boundary conditions:

$$w(x, t) = \sum_{i=1}^N q_i(t) \phi_i(x), \quad (10)$$

where $q_i(t)$ are the time-dependent generalised coordinates and $\phi_i(x)$ are appropriate basis functions. For the clamped-clamped beam, linear undamped mode shapes are assumed (see Blevins, 1979):

$$\begin{aligned} \phi_i(x) &= \cosh \lambda_i x - \cos \lambda_i x \\ &\quad - \sigma_i (\sinh \lambda_i x - \sin \lambda_i x). \end{aligned} \quad (11)$$

where λ_i are the roots of the characteristic equation

$$\cos \lambda \cosh \lambda = 1, \quad (12)$$

and σ_i is given by

$$\sigma_i = \frac{\cosh \lambda_i - \cos \lambda_i}{\sinh \lambda_i - \sin \lambda_i}. \quad (13)$$

The mode-shapes are normalised such that:

$$\int_0^1 \phi_i \phi_j dx = \begin{cases} 1, & \text{if } i = j, \\ 0, & \text{if } i \neq j. \end{cases} \quad (14)$$

Due to the symmetric electrode layout of the resonator, and a bias voltage V_{dc} applied to each of the two electrodes (see (3)), oscillations of the resonator take place around its undeformed ($w = 0$) position. No static transverse deflection of the resonator will take place, only dynamic deflection. For this reason, a single-mode discretization has been found to capture the nonlinear dynamic behaviour sufficiently well (this will become clear from Section 4). In case of a one-sided electrode layout, see for instance Abdel-Rahman *et al.* (2002) and Younis and Nayfeh (2003), a single-mode discretization has been found not to suffice.

To derive a single-mode Galerkin discretization for the PDE, consider a single-mode version of (10), $w(x, t) = q_1(t) \phi_1(x)$, for which λ_1 and σ_1 are found from Blevins (1979):

$$\lambda_1 = 4.73004074, \quad \text{and} \quad \sigma_1 = 0.982502215. \quad (15)$$

In order to avoid division by zero in the electrostatic force term, (7) is multiplied by the common denominator of the right-hand side: $(1 - w)^2(1 + w)^2 = (1 - w^2)^2$.

The procedure to arrive at the discretized model consists of substituting $w(x, t) = q_1(t)\phi_1(x)$ into the pre-multiplied version of (7). The residual, obtained in this way, is requested to be orthogonal to the single-mode approximation. This is achieved by multiplying the residual by ϕ_1 and integrating from 0 to 1 over x . This results in the single degree-of-freedom nonlinear ordinary differential equation:

$$\begin{aligned} & (\ddot{q}_1 + c_d \dot{q}_1 + \lambda_1^4 q_1) \\ & \times (1 - 2q_1^2 \int_0^1 \phi_1^4 dx + q_1^4 \int_0^1 \phi_1^6 dx) \\ & - c_{nl} q_1^3 \int_0^1 (\phi_1')^2 dx \\ & \times (\int_0^1 \phi_1'' \phi_1 dx - 2q_1^2 \int_0^1 \phi_1'' \phi_1^3 dx + q_1^4 \int_0^1 \phi_1'' \phi_1^5 dx) \\ & = c_f \left\{ (\int_0^1 \phi_1 dx + 2q_1 + q_1^2 \int_0^1 \phi_1^3 dx) V_1^2(t) \right. \\ & \quad \left. - (\int_0^1 \phi_1 dx - 2q_1 + q_1^2 \int_0^1 \phi_1^3 dx) V_2^2(t) \right\}. \end{aligned} \quad (16)$$

3.4 Numerical Approach

The simulation model for the clamped-clamped beam consists of a state-space description of the second-order nonlinear differential equation (16), $\dot{\mathbf{x}} = \mathbf{f}(\mathbf{x}, t)$, where the state column is defined by $\mathbf{x} = [q_1 \dot{q}_1]^T$. The steady-state nonlinear dynamic behaviour of the model is investigated by applying numerical collocation and continuation techniques, available in the package AUTO (Doedel *et al.*, 1998). Periodic solutions (resonator vibrations) for various excitation frequencies f can be determined. The method is suitable for general nonlinear systems, in contrast to perturbation techniques, applied in, for instance, Younis and Nayfeh (2003). Results will be discussed in Section 4.

4 Results

Numerical simulations have been performed using the approach described in Section 3.4. Parameter values for the model have been derived from the physical dimensions and material properties of the resonator and are listed in Table 1. Furthermore, damping has been implemented by means of a non-dimensional equivalent linear damping coefficient ξ , whose value is obtained from Mestrom *et al.* (2007). Due to operation in vacuum, the system is very weakly damped. The equivalent linear damping coefficient ξ would translate to a Q -factor of $Q = 1/(2\xi) = 6250$.

4.1 Frequency Hysteresis

In Figs. 6 and 7, simulated amplitude-frequency curves are depicted for a bias voltage of $V_{dc} = 70$ V and ac excitation values of $V_{ac} = 70$ and 139 mV, respectively. The figures show the maximum non-dimensional amplitude of the mid-point of the beam

Table 1. Numerical values for the parameters in the model (7).

Parameter	Value	Unit
E	131.1×10^9	N/m ²
ρ	2.330×10^3	kg/m ³
b	1.4×10^{-6}	m
h	4.0×10^{-6}	m
l	48.4×10^{-6}	m
d	0.330×10^{-6}	m
ξ	8.0×10^{-5}	–

w_{max} versus the excitation frequency. Furthermore, stable and unstable parts of the numerical amplitude-frequency curves are indicated. Solid curves correspond to stable periodic solutions, whereas dashed curves correspond to unstable ones (not seen in measurements). The transition between stable and unstable branches of periodic solutions is characterized by cyclic fold (cf) bifurcations (see for instance Thomsen, 2003).

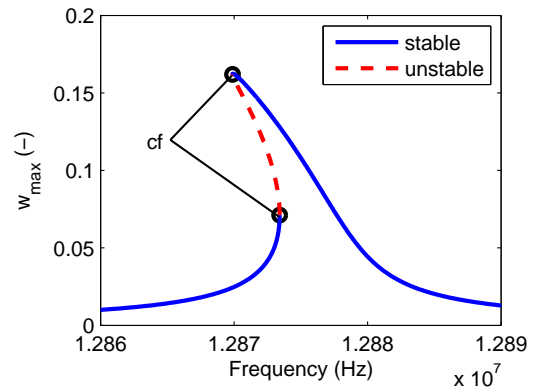


Figure 6. Simulated amplitude-frequency curve, $V_{ac} = 70$ mV.

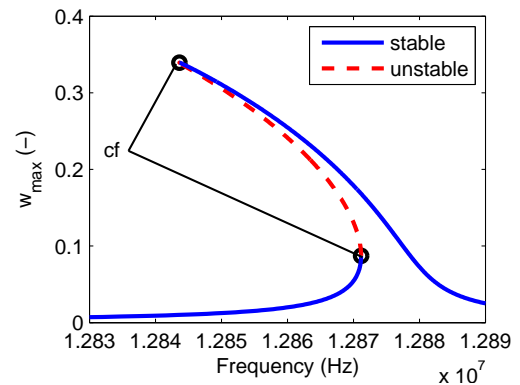


Figure 7. Simulated amplitude-frequency curve, $V_{ac} = 139$ mV.

The cyclic fold bifurcations in Figs. 6 and 7 are responsible for sudden jumps in the measured amplitude-frequency behaviour during frequency sweeps (Figs. 3 and 4). This can be understood by considering the numerical amplitude-frequency curves. Starting from a frequency below the fundamental resonance, the system's response follows the stable low amplitude branch if the excitation frequency is increased until the lower cf point. From there, an increase in frequency makes

the system ‘jump’ to the upper branch of stable solutions. This jump is clearly observed in the experimental curves (see Figs. 3 and 4). An analogous explanation holds for the sweep down behaviour by considering the upper of bifurcation point.

By comparing the numerical curves with the experimental ones, it can be seen that a good qualitative match has been obtained. A quantitative comparison of the results in terms of the output voltage V_{out} is still in progress and clearly depends on a proper identification of the physical parameters. Furthermore, under a multi-mode approximation ($N > 1$ in (10)–(14)), results do not change significantly in the frequency range of interest.

4.2 Hardening and Softening

Depending on the excitation parameters (V_{dc} and V_{ac}), the dynamic response may show hardening or softening nonlinear behavior. Since the excitation contains $V_1^2(t)$, see (3), the amplitude of the harmonic excitation (at frequency f) has a value equal to $2V_{dc}V_{ac}$. In Fig. 8, hardening and softening behaviour is depicted for the situation where $V_{dc}V_{ac}$ is kept constant at 9.73 V^2 , which corresponds to $V_{dc} = 70 \text{ V}$ and $V_{ac} = 139 \text{ mV}$. In Fig. 8, the amplitude-frequency curves are depicted

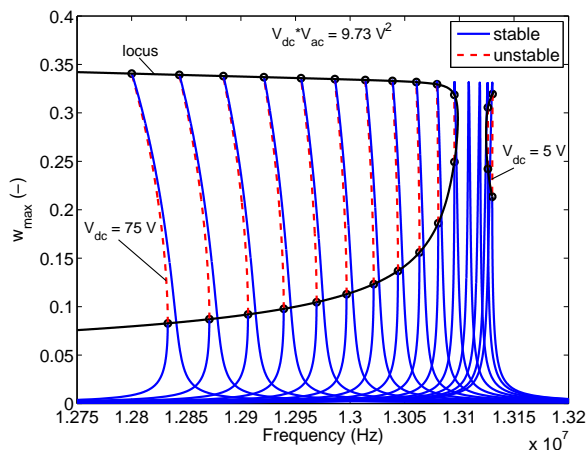


Figure 8. Hardening and softening nonlinearities, depending on the excitation values. Also the loci of cf points are indicated.

for bias voltages ranging from 5 to 75 V. For low bias voltage values, the resonance peak bends to higher frequencies. Here, the hardening effect due to midplane stretching dominates the softening effect due to electrostatic excitation. For high bias voltages, the peak bends to lower frequencies. Here, it is the other way around: the electrostatic softening dominates the hardening due to midplane stretching. At intermediate values, a nearly linear response can be seen. The reason for this is the balance between the mid-plane stretching nonlinear effect (hardening) and the electrostatic nonlinear effect (softening). This has also been reported in Younis and Nayfeh (2003). Moreover, loci of cf points have been calculated and are indicated in Fig. 8.

4.3 Subharmonic Resonance

The model is also capable of predicting the 1/2 subharmonic resonance, for which the experimental result was depicted in Fig. 5. The simulation result for $V_{dc} = 70 \text{ V}$ and $V_{ac} = 350 \text{ mV}$ is depicted in Fig. 9. In this case, the non-dimensional damping coefficient is slightly lower than in Table 1, namely $\xi = 4.8 \times 10^{-5}$. The subharmonic resonance peak is

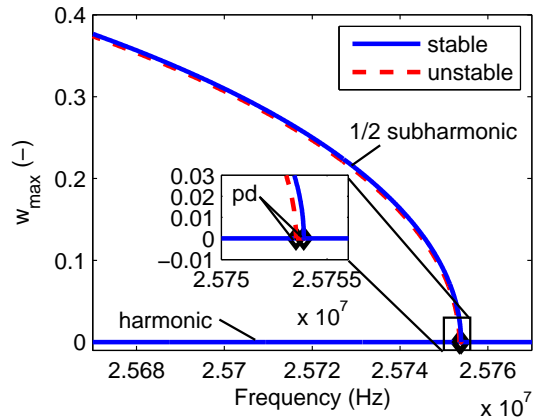


Figure 9. Simulated 1/2 subharmonic resonance.

initiated by two so-called period doubling bifurcations (Thomsen, 2003) near twice the non-dimensional fundamental frequency, denoted by ‘pd’ the inset in Fig. 9.

5 Conclusions and Future Work

The proposed first-principles based model for the clamped-clamped beam resonator captures the experimentally observed nonlinear dynamic behaviour of the resonator and allows for fast and accurate prediction. As a result, it will enable parameter studies and investigation of different design and layout aspects for microelectromechanical resonators. In this paper, a qualitative/quantitative correspondence between numerical and experimental results has been obtained.

Future work will consist of further experimental verification of the current reduced-order model. Based on the assessment of the accuracy of the assumptions made, future work will incorporate improvement and extensions of the model. Firstly, this will comprise the inclusion of fringing field effects in the electrostatic actuation and a more in-detail description of the various damping contributions in the system. Secondly, material nonlinear effects and thermal effects will be included. Moreover, oscillator design aspects and the effect of different resonator layouts will be addressed, in order to predict resonator performance and to derive guidelines for optimal layout.

Acknowledgements

Experimental support of NXP Semiconductors, Eindhoven, the Netherlands, is gratefully acknowledged.

References

- Abdel-Rahman, E. M., M. I. Younis and A. H. Nayfeh (2002). Characterization of the mechanical behavior of an electrically actuated microbeam. *J. Micromech. Microeng.* **12**(6), 759–766.
- Batra, R. C., M. Porfiri and D. Spinello (2006a). Capacitance estimate for electrostatically actuated narrow microbeams. *Micro Nano Lett.* **1**(2), 71–73.
- Batra, R. C., M. Porfiri and D. Spinello (2006b). Electromechanical Model of Electrically Actuated Narrow Microbeams. *J. Microelectromech. Syst.* **15**(5), 1175–1189.
- Blevins, R. D. (1979). *Formulas for Natural Frequency and Mode Shape*. Van Nostrand Reinhold, London.
- Doedel, E., A. R. Champneys, T. F. Fairgrieve, Y. A. Kuznetsov, B. Sandstede and X. Wang (1998). *AUTO97: Continuation and Bifurcation Software for Ordinary Differential Equations (with HomCont)*, Technical Report. Concordia University.
- Foulgoc, B. L., T. Bourouina, O. L. Traon, A. Bosseboeuf, F. Marty, C. Breluzeau, J. P. Grandchamp and S. Masson (2006). Highly decoupled single-crystal silicon resonators: an approach for the intrinsic quality factor. *J. Micromech. Microeng.* **16**(6), S45–S53.
- Kaajakari, V., T. Mattila, A. Oja and H. Seppä (2004). Nonlinear Limits for Single-Crystal Silicon Microresonators. *J. Microelectromech. Syst.* **13**(5), 715–724.
- Lifshitz, R. and M. L. Roukes (2000). Thermoelastic damping in micro- and nanomechanical systems. *Phys. Rev. B* **61**(8), 5600–5609.
- Mattila, T., J. Kiihamäki, T. Lamminmäki, O. Jaakkola, P. Rantakari, A. Oja, H. Seppä, H. Kattelus and I. Tittonen (2002). A 12 MHz micromechanical bulk acoustic mode oscillator. *Sens. Actuators A* **101**(1–2), 1–9.
- Mestrom, R. M. C., R. H. B. Fey, J. T. M. van Beek, K. L. Phan and H. Nijmeijer (2007). Modelling the dynamics of a MEMS resonator: Simulations and experiments, *in press*. *Sens. Actuators A*.
- Nayfeh, A. H. and M. I. Younis (2004). Modeling and simulations of thermoelastic damping in microplates. *J. Micromech. Microeng.* **14**(12), 1711–1717.
- Nguyen, C. T.-C. (2005). Vibrating RF MEMS technology: fuel for an integrated micromechanical circuit revolution?. *Procs. Transducers '05* pp. 243–246.
- Nguyen, C. T.-C. (2007). MEMS Technology for Timing and Frequency Control. *IEEE Trans. Ultrason. Ferr.* **54**(2), 251–270.
- Senturia, S. D. (2001). *Microsystems Design*. Kluwer Academic Publishers.
- Thomsen, J. J. (2003). *Vibrations and Stability; Advanced Theory, Analysis and Tools*. 2nd ed. Springer Verlag, Berlin.
- Tilmans, H. A. C. and R. Legtenberg (1994). Electrostatically driven, vacuum-encapsulated polysilicon resonators; Part II: theory and performance. *Sens. Actuators A* **45**(1), 67–84.
- Tilmans, H. A. C., M. Elwenspoek and J. H. J. Fluitman (1992). Micro resonant force gauges. *Sens. Actuators A* **30**(1), 35–53.
- Younis, M. I. and A. H. Nayfeh (2003). A Study of the Nonlinear Response of a Resonant Microbeam to an Electric Actuation. *Nonlin. Dynam.* **31**(1), 91–117.